

Core Losses Under the DC Bias Condition Based on Steinmetz Parameters

Journal Article

Author(s):

Mühlethaler, Jonas; Biela, Jürgen ; Kolar, Johann W. ; Ecklebe, Andreas

Publication date:

2012-02

Permanent link:

<https://doi.org/10.3929/ethz-b-000039067>

Rights / license:

[In Copyright - Non-Commercial Use Permitted](#)

Originally published in:

IEEE Transactions on Power Electronics 27(2), <https://doi.org/10.1109/TPEL.2011.2160971>

Core Losses under DC Bias Condition based on Steinmetz Parameters

Jonas Mühlethaler, *Student Member, IEEE*, Jürgen Biela *Member, IEEE*, Johann Walter Kolar *Fellow, IEEE*, and Andreas Ecklebe *Member, IEEE*

Abstract—The calculation of core losses in inductive components is a difficult and not yet entirely solved problem. In particular it is impossible to predict the influence of a DC premagnetization on the losses without extensive measurements. For this work, different materials have been tested to gain information how core losses are influenced by a premagnetization. Measurements on molypermalloy powder, silicon steel, nanocrystalline material, and ferrite cores have been performed. Of the tested materials, a premagnetization mainly influences losses in ferrites and nanocrystalline materials, whereas the influence of a premagnetization in molypermalloy powder cores, and cores of silicon steel is less pronounced. The *Steinmetz Premagnetization Graph* (SPG) that shows the dependency of the Steinmetz parameters (α , β and k) on premagnetization is introduced. This permits the calculation of core losses under DC bias conditions. Such graphs are given for different materials and different operating temperatures. In addition, a detailed description of the test system is given, as high accuracy is crucial.

Index Terms—Core losses, ferrite, Steinmetz, DC bias.

I. INTRODUCTION

THE calculation of core losses in inductive components is a difficult and not yet entirely solved problem. Particularly, the influence of a DC bias on the losses is not entirely clarified. The most used equation that characterizes core losses is the power equation [1]¹

$$P_v = k f^\alpha \hat{B}^\beta \quad (1)$$

where \hat{B} is the peak induction of a sinusoidal excitation with frequency f , P_v is the time-average power loss per unit volume, and k , α , β are material parameters. The equation is often referred to as the Steinmetz equation, named after Charles P. Steinmetz, who proposed a similar equation, without the frequency dependence, in 1892 [2]. The material parameters k , α , and β are accordingly referred to as the Steinmetz parameters. They are valid for a limited frequency and flux density range. Unfortunately, the Steinmetz equation is only valid for sinusoidal

excitation. This is a huge drawback, because in power electronics applications the material is mostly exposed to non sinusoidal flux waveforms.

Different approaches have been developed to overcome this limitation and determine losses for a wider variety of waveforms. The approaches can be classified into the following categories:

- 1) Improvements of the Steinmetz Equation (1).
- 2) Calculation of the losses with a loss map that is based on measurements. This loss map stores the loss information for different operating points, each described by the flux density ripple ΔB , the frequency f , the temperature T , and a DC bias H_{DC} (e.g. in [3]–[5]).
- 3) Methods to determine core losses based on breaking up the total loss into loss components, i.e. hysteresis losses, classical eddy current losses, and "excess losses" [6], [7].
- 4) Hysteresis models such as Preisach and Jiles-Atherton used for the calculation of core losses.

One of the approaches based on an improved Steinmetz equation is derived in [8], [9], and [10]. The analysis in [8] is motivated by the fact that the loss due to domain wall motion has a direct dependency of dB/dt . As a result, a modified Steinmetz equation is proposed. In [9] the approach is further improved and in [10] a method how to deal with minor hysteresis loops is presented and some minor changes on the equation are made. The approach of [8], [9], and [10] leads to the improved Generalized Steinmetz Equation (iGSE)

$$P_v = \frac{1}{T} \int_0^T k_i \left| \frac{dB}{dt} \right|^\alpha (\Delta B)^{\beta-\alpha} dt \quad (2)$$

where ΔB is peak-to-peak flux density and

$$k_i = \frac{k}{(2\pi)^{\alpha-1} \int_0^{2\pi} |\cos \theta|^{\alpha} 2^{\beta-\alpha} d\theta}. \quad (3)$$

The parameters k , α , and β are the same parameters as used in the Steinmetz equation (1). The iGSE is capable of calculating losses of any flux waveform, without requiring extra characterization of material parameters beyond the parameters for the Steinmetz equation. This approach is widely applied [11], [12]. Nevertheless, the iGSE has a drawback: it neglects the fact that core losses vary under DC bias conditions, i.e. the Steinmetz parameters change under DC bias condition.

J. Mühlethaler and J. W. Kolar are with the Power Electronic Systems Laboratory, ETH Zurich, www.pes.ee.ethz.ch, Email: muehlethaler@lem.ee.ethz.ch and kolar@lem.ee.ethz.ch

J. Biela is with the Laboratory for High Power Electronic Systems, ETH Zurich, www.hpe.ee.ethz.ch, Email: jbiela@ethz.ch

A. Ecklebe is with ABB Switzerland Ltd., Corporate Research, CH-5405 Baden-Dättwil, Email: andreas.ecklebe@ch.abb.com

¹To have units work out properly, the Steinmetz equation should actually be written $P_v = k \left(\frac{f}{f_{ref}} \right)^\alpha \left(\frac{\hat{B}}{B_{ref}} \right)^\beta$. However, it is very common to use (1) and implicitly assume $B_{ref} = 1$ T and $f_{ref} = 1$ Hz (or another set of units).

In many power electronics applications magnetic components are biased with a DC or low-frequency pre-magnetization, e.g. in Switched-Mode Power Supplies (SMPS). Within SMPS circuits, magnetic components that are operating under DC bias conditions are commonly used and are often among the largest components. Many publications have shown that the influence of DC bias on the material properties can not be neglected [8], [13]–[18]. An approach how to handle DC bias losses is described in [3], [4] and [5]. There, losses are calculated with a loss map that is based on measurements. This loss map stores the loss information for many operating points, each described by the flux ripple ΔB , the frequency f , and a DC bias H_{DC} . It is explained, how this loss map can be used to calculate iron losses of inductors employed in power electronic systems. One parameter in the loss map is the DC premagnetization, thus the loss increase due to DC bias is considered in this approach. However, extensive measurements are necessary to build the loss map. Another approach how to consider DC bias losses is introduced in [13]: the effect of a DC bias is modeled by the given ratio between losses with and without DC bias for different DC bias levels H_{DC} and different AC flux densities. This ratio is called the displacement factor DPF. In [13] a graph that shows the DPF is given for the material ferrite N87 from EPCOS. In [8] an empirical formula that describes the DPF is given (though it is not named DPF). According to [8], [13] the DPF does not depend on the frequency f and can be described as a function of the AC flux density and the DC bias H_{DC} . A similar approach is suggested in [14], but according to [14] the DPF does not depend on the AC flux density. The influence of the frequency on the DPF has not been discussed. The approaches of [8], [13], [14] have in common that a factor is introduced by which the calculated losses have to be multiplied to take a premagnetization into consideration. In other words, the parameter k of (1) (or k_i of (2)) is multiplied by the DPF and therewith becomes dependent on \hat{B} (or ΔB).

This work proposes a new approach how to describe core losses under DC bias condition. A graph that shows the dependency of the Steinmetz parameters (α , β and k) on premagnetization is introduced in Section IV. This enables the calculation of losses via the Steinmetz equation (1) or the iGSE (2) using appropriate Steinmetz parameters. A core loss measurement test setup has been built for this work and is presented in Section II. The accuracy of the system is analyzed in Section III.

II. TEST SETUP TO MEASURE CORE LOSSES

To perform measurements, the best measurement technique has to be selected first. In [19] different methods are compared. The B-H Loop Measurement has been evaluated as the most suitable. Amongst other advantages, this technique offers rapid measurement (compared to other methods, e.g. calorimetric measurement), copper losses are not measured, and a good accuracy. In Section

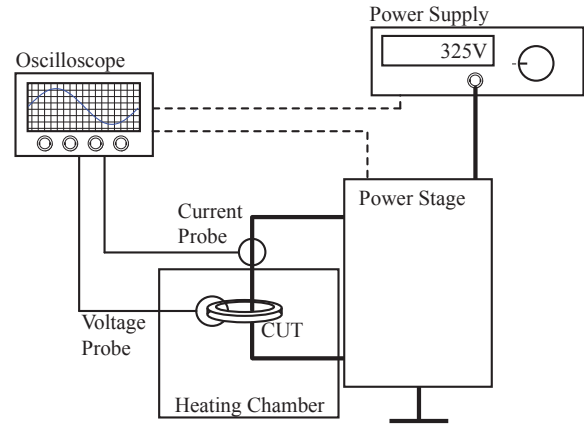


Fig. 1. Overview of the test system.

TABLE I
MEASUREMENT EQUIPMENT

Oscilloscope	LeCroy WaveSurfer 24MXs-A
Current Probe	LeCroy AP015
Heating Chamber	Binder ED53
Power Supply	Xantrex XTR 600-1.4
Power Stage	0 – 450 V 0 – 25 A 0 – 200 kHz

III the accuracy is analyzed in detail. The principles are as follows: two windings are placed around the Core Under Test (CUT). The sense winding (secondary winding) voltage v is integrated to sense the core flux density B

$$B(t) = \frac{1}{N_2 \cdot A_e} \int_0^t v(\tau) d\tau \quad (4)$$

where N_2 is the number of sense winding turns and A_e the effective core cross section of the CUT. The current in the excitation winding (primary winding) is proportional to the magnetic field strengths H

$$H(t) = \frac{N_1 \cdot i(t)}{l_e} \quad (5)$$

where N_1 is the number of excitation winding turns and l_e the effective magnetic path length of the CUT. The loss per unit volume is then the enclosed area of the B-H loop, multiplied by the frequency f^2

$$\frac{P}{V} = f \oint H dB. \quad (6)$$

The selected approach is widely used [4], [10], [20], [21]. The test system consists of an oscilloscope, a power supply, a heating chamber, and a power stage, as illustrated in

²The core loss per unit volume is

$$\begin{aligned} \frac{P}{V} &= \frac{f \int_0^T i_1(t) \frac{N_1}{N_2} v_2(t) dt}{A_e l_e} = \frac{f \int_0^T H(t) l_e \frac{1}{N_1} N_1 A_e \frac{dB(t)}{dt} dt}{A_e l_e} \\ &= f \int_{B(0)}^{B(T)} H(B) dB = f \oint H dB, \end{aligned}$$

where $\frac{N_1}{N_2} v_2(t)$ is the sense winding voltage transformed to the primary side.

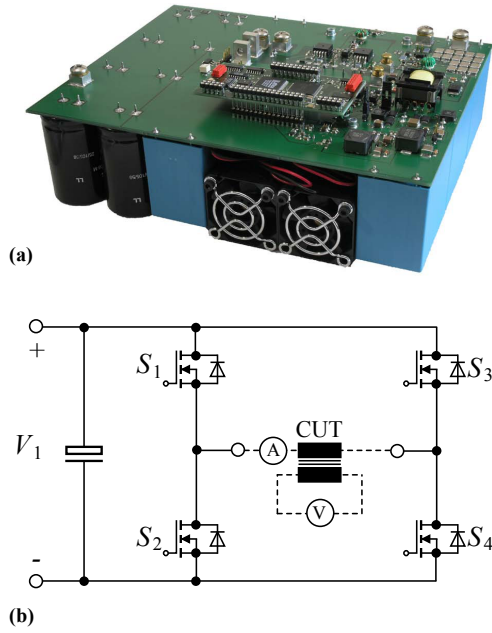


Fig. 2. Power stage (a) photograph, (b) simplified schematic.

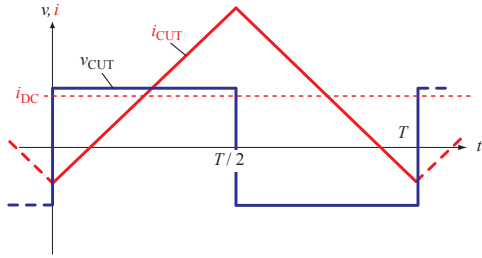


Fig. 3. Current and voltage waveforms of the CUT.

Fig. 1. It is controlled by a MATLAB program running on the oscilloscope under Microsoft Windows. In Table I the used equipment is listed. In Fig. 2 a photograph (a) and the simplified schematic (b) of the power stage is shown. In Table II the most important components employed in the power stage are listed. The power stage is capable of a maximal input voltage of 450 V, output current of 25 A and a switching frequency of up to 200 kHz. With the power stage, it is possible to achieve a rectangular voltage shape across the CUT that leads to a triangular current shape including a DC bias (if desired). This behavior is illustrated in Fig. 3. To control the DC current, the current is sensed by a DC current transducer. A low frequency sinusoidal excitation is also possible; for this an output filter has been designed to achieve a sinusoidal current/voltage shape for frequencies up to 1 kHz.

III. ACCURACY OF THE MEASUREMENT SYSTEM

The different aspects that influence the accuracy of the measurements are given in the following.

TABLE II
POWER STAGE COMPONENTS

Power MOSFETs	IXYS IXFB82N60P
Gate Driver	IXYS IXDD414SI
Capacitors	Electrolytic: 2.75 mF Foil: 360 μ F Ceramic: 3.86 μ F
DSP	TI TMS320F2808
Current Sensor	LEM LTS 25-NP
Fan	San Ace 40 GE

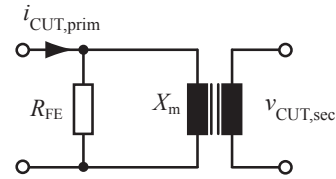


Fig. 4. Equivalent circuit of the CUT.

A. Phase Shift Error of Voltage and Current Measurement

The error due to an inaccurate measurement of the voltage and current phase displacement can be quantified as [22]

$$E = 100 \cdot \frac{\cos(\zeta + \phi) - \cos \zeta}{\cos \zeta}, \quad (7)$$

where E is the relative error in % of the measured core losses, ζ is the actual phase shift between the sense winding output voltage and the excitation winding current, and ϕ is the error in the measurement of ζ . Measurements have shown that ϕ depends linearly on the frequency. In other words, ϕ originates from a delay time T_d that is independent of the frequency. This delay time T_d can be measured with a rectangular current shape through a low inductance shunt, and with it the delay time can be compensated. The main cause of the delay time T_d is the current probe.

In Section IV measurements with the material ferrite N87 from EPCOS (core part number: B64290L22X87) are presented; therefore a short discussion about phase shift accuracy is given on the example of this core. This accuracy discussion is similar to the discussion presented in [17]. In Fig. 4 a simplified equivalent circuit of the Core Under Test (CUT) is given. Winding losses and leakage inductance are assumed to be negligible. The reactance X_m can be calculated as

$$X_m = \omega A_L N_1^2, \quad (8)$$

where A_L is the inductance factor, N_1 is the number of primary winding turns, and $\omega = 2\pi f$ is the angular frequency. Hence, for the CUT ($A_L = 2560$ nH [23], $N_1 = 10$) and a frequency $f = 100$ kHz the reactance is $X_m = 160.8 \Omega$. At the operating point $\Delta B = 100$ mT, $f = 100$ kHz, and $T = 40^\circ \text{C}$ losses of $P_{\text{Loss}} = 0.2$ W are expected (from material data sheet [23]). With this information, the equivalent resistor R_{FE} that represents

the core losses can be calculated

$$R_{FE} = \frac{V_{rms}^2}{P_{Loss}} = \frac{\left(N_1 A_e \omega \frac{\Delta B}{2\sqrt{2}}\right)^2}{P_{Loss}}, \quad (9)$$

where A_e is the equivalent core cross section. For the CUT and operating point, the resistor R_{FE} is 2.26 k Ω . Now, the angle ζ can be calculated as

$$\zeta = \arctan \frac{R_{FE}}{X_m} = 85.9^\circ \quad (10)$$

An uncompensated delay time T_d would result in a phase shift error of voltage and current measurement of

$$\phi = f \cdot T_d \cdot 360^\circ. \quad (11)$$

When (11) is inserted in (7) and then solved for T_d , a tolerable uncompensated delay time for a desired accuracy is derived; e.g. for an accuracy of $\pm 3\%$, an uncompensated delay time of ± 3.5 ns at 100 kHz and $\zeta = 85.9^\circ$ would be tolerable. Measurements have shown that the delay time compensation leads to lower residual delay times; although a quantification is difficult. With a realistic delay time compensation to an accuracy of ± 1.5 ns, and with an expected system accuracy (only phase shift consideration) of $\pm 4\%$, measurements of materials up to an angle of $\zeta = 88.7^\circ$ (at $f = 100$ kHz) can be performed. At lower frequency measurements the permitted angle ζ increases for the same accuracy constraint; e.g. at 20 kHz, for an accuracy of $\pm 4\%$, measurements up to an angle of $\zeta = 89.7^\circ$ are permitted. All measurements presented in the next sections are within this range.

The system has one drawback related to the phase shift: the measurement of gapped cores (or low permeability cores) is difficult because the angle ζ substantially increases in this situation. A detailed analysis together with a new method of how gapped cores could be measured is introduced in [18]. A measurement method that improves core loss measurement for very high frequencies (1 MHz - 50 MHz) is proposed in [24]. Although the focus of [24] are measurements at very high frequencies, the method could be used to improve the loss measurement of gapped cores. However, for the work in hand only un-gapped cores have been measured.

B. Equipment Accuracy

A typical magnitude/frequency characteristic of the current probe has been provided by the current probe manufacturer LeCroy, from which an AC accuracy of 3% could be extracted. Together with the accuracy of the passive probe (attenuation accuracy of 1%) and the accuracy of the oscilloscope itself (1.5% that originates amongst others from the limited vertical resolution of 8 bit), an equipment accuracy of $\leq |\pm 5.6\%|$ is derived.

C. Capacitive Coupling

Capacitive currents may result in errors and must therefore be avoided. The typical capacitances that are present in windings are

- capacitance between the primary and secondary winding (inter capacitance),
- self capacitance between turns of a winding (intra capacitance),
- and capacitance between the windings and the magnetic core.

According to [25], the inter and intra capacitances increase when the core is grounded; thus the core should not be grounded. Generally, the inter and intra capacitances increase with increasing area between the windings and decrease with distance between the windings. To decrease the inter capacitance, a separation of the primary and secondary windings is favorable; although a separation of the windings avoids an absolute uniform winding distribution around the core (ideally, the primary winding should be distributed uniformly around the core to achieve a homogenous flux density distribution). Another important aspect of the winding arrangement is the chosen number of turns of the primary winding. Even with the use of favorable winding layout, some ringing in current and voltage is inevitable. Fewer turns are more favorable for two reasons: this additionally decreases parasitic capacitances, and, because the current for the same magnetic operating point is higher, capacitive currents are relatively lower compared to (desired) inductive currents.

D. Temperature

An important aspect is that the temperature of the CUT is defined and constant. To keep the temperature constant, the test system performs the measurement automatically (starts excitation, controls current, regulates flux (ΔB), triggers the oscilloscope, reads values). With such an automated measurement system, a working point is rapidly measured and the losses do not heat the core in the short measurement period.

E. Comparative Measurement and Conclusion

Comparative measurements with the power analyzer *Norma D6100* have been performed to confirm the accuracy. The power analyzer is connected to measure the excitation winding current and the sense winding voltage to obtain core losses [19]. The results in the performed working points matched very well. The deviation between the results of the test system and of the power analyzer was always $\leq |\pm 4\%|$ (up to 100 kHz).

From the equipment accuracy ($\leq |\pm 5.6\%|$) and the phase shift accuracy ($\leq |\pm 4\%|$), a system accuracy of $\leq |\pm 9.8\%|$ is calculated. However, based on the results of the comparative measurements, it can be said that the reached accuracy is higher.

As a conclusion, a test system has been built up that performs the measurements quickly and leads to sufficiently accurate results.

IV. CORE LOSSES OF FERRITES UNDER DC BIAS CONDITION

In this section, measurement results are presented and a new approach to describe core losses under DC bias

conditions is introduced that is based on a graph that shows the dependency of the Steinmetz parameters (α , β and k) on premagnetization. This is done on the example of the material ferrite N87 from EPCOS (core part number B64290L22X87 [23]). In Fig. 5 the core losses and in Fig. 6 the core losses normalized to the losses P_0 at zero premagnetization are shown for different DC bias values. In Fig. 7 the losses are plotted as a function of the frequency f and in Fig. 8 the losses are plotted as a function of the peak-to-peak flux density ΔB , with and without DC bias. To describe the losses via the Steinmetz equation (1) or the iGSE (2) is the most common method, hence improvements of this method would be most beneficial for design engineers. As the iGSE (2) is more suitable for the description of core losses in power electronic applications, in all following considerations the three discussed parameters are α , β , and k_i of the iGSE (α , β are the same as in (1), while k_i is described in (3)). For the applied waveform as illustrated in Fig. 3 (symmetric triangular current/flux shape) (2) leads to

$$P_v = k_i(2f)^\alpha \Delta B^\beta. \quad (12)$$

When core losses are plotted with logarithmic axes, where the x-axis represents the frequency and the y-axis represents the power loss, approximately straight line are drawn (cf. Fig. 7). This is because the losses follow a power function as e.g. the laws stated in (1) and the iGSE (2) are. The parameter α represents the slope of the curve in this plot. The same can be said when the frequency f is kept constant and ΔB is varied; hence, the use of a power function with variable ΔB is justified as well (cf. Fig. 8). The parameter β represents the slope of the curve in this plot. When a core is under DC bias condition, the losses over a wide range of H_{DC} still can be described with the Steinmetz equation (1) or the iGSE (2), i.e. the losses still follow the power equation stated by Steinmetz (cf. Fig. 7 and Fig. 8). However, for very high values of H_{DC} and high flux densities ΔB the use of a power function is not appropriate anymore (cf. Fig. 8, curve for $H_{DC} = 80$ A/m). This is due to saturation effects. The curve for $H_{DC} = 50$ A/m has been determined as the last one that can be considered as an approximate straight line over a wide flux density range. For most applications it is not desired to operate at higher DC bias levels; hence, the majority of inductive components are operated in a range where the losses still follow the power equation stated by Steinmetz.

As described above the Steinmetz parameters must be adjusted according to the DC bias present. As will be shown in the following, a DC bias causes changes in the Steinmetz parameters β and k_i , but not in the parameter α .

- The losses change when ΔB and frequency f are kept constant and the DC bias H_{DC} is varied (cf. Fig. 5). Thus, the Steinmetz parameter k_i depends on the DC bias H_{DC} ($k_i = f(H_{DC})$).
- When the frequency f is kept constant, the factor by

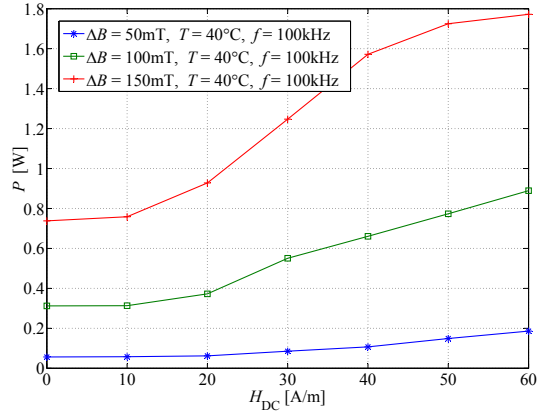


Fig. 5. Core losses under DC bias conditions (ferrite N87; measured on R42 core), $f = 100$ kHz, $T = 40^\circ\text{C}$.

which the losses increase due to a premagnetization H_{DC} differs for different ΔB (cf. Fig. 6). Thus, the Steinmetz parameter β depends on the premagnetization H_{DC} as well ($\beta = f(H_{DC})$). The slopes of the curves in Fig. 8 represent the parameter β . As can be seen the curve for $H_{DC} = 20$ A/m is slightly steeper compared to the curve of $H_{DC} = 0$ A/m, though the difference is very little. However, a small change in β already considerably influences the core losses, as one can see when comparing with Fig. 6. It should be again pointed out that it is only valid to define a β within the range of H_{DC} where the logarithmic plotted losses lead to an approximate straight line (cf. Fig. 8).

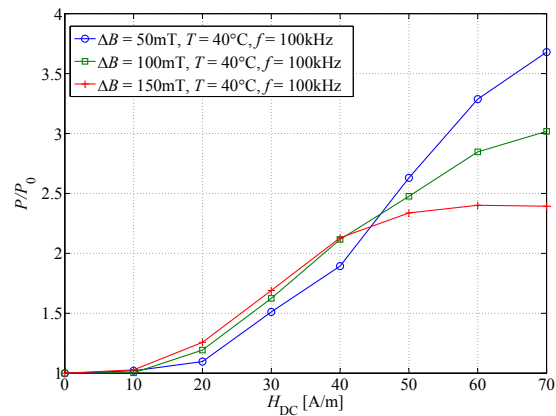


Fig. 6. Core losses under DC bias conditions, normalized to losses P_0 at zero premagnetization (ferrite N87; measured on R42 core), $f = 100$ kHz, $T = 40^\circ\text{C}$.

- According to [13], the influence of a DC bias does not depend on the measurement frequency f . This has been confirmed for frequencies up to 100 kHz. As can be seen in Fig. 7, at a constant ΔB , the factor by which the losses increase due to a premagnetization H_{DC} is the same for different frequencies f (the slopes of the curves remain the same). Hence, the Steinmetz parameter α is in this

frequency range independent of the premagnetization H_{DC} ($\alpha = \text{const.}$). The fact that α is constant has been confirmed to frequencies up to 100 kHz, no measurements above this frequency have been performed, hence no information can be given as to whether and up to which frequency α is constant.

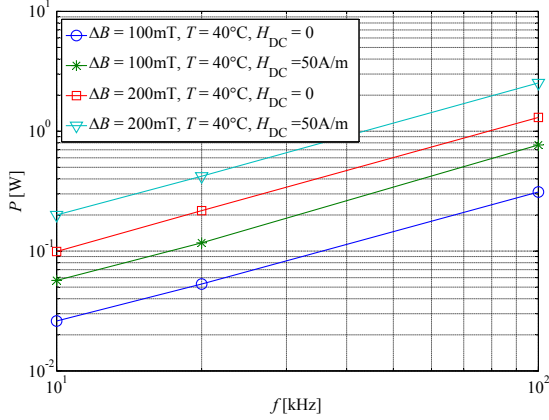


Fig. 7. Core losses vs. frequency (ferrite N87; measured on R42 core), $T = 40^\circ\text{C}$.

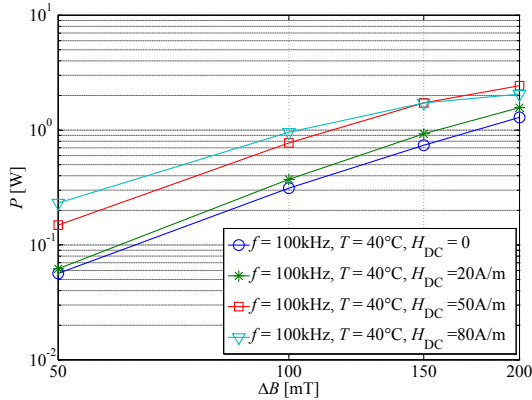


Fig. 8. Core losses vs. flux density (ferrite N87; measured on R42 core), $T = 40^\circ\text{C}$.

Next, at each tested DC bias level the Steinmetz parameters have been extracted. A least square algorithm has been implemented that fits measured losses with calculated data by minimizing the relative error at 3 different values of ΔB , each measured at two frequencies. The markers on top of the curves in Fig. 9 represent these values. As not only the Steinmetz parameters at discrete operating points are of interest, a curve fitting algorithm has been implemented to extract the dependencies $\beta = f(H_{DC})$ and $k_i = f(H_{DC})$. Its derivation is discussed in Appendix B.

For the material N87 from EPCOS the dependencies $\beta = f(H_{DC})$ and $k_i = f(H_{DC})$ are given in Fig. 9, and normalized to β_0 and k_{i0} in Fig. 10. β_0 and k_{i0} are the Steinmetz parameters at zero premagnetization. We call the graph illustrated in Fig. 10 the *Steinmetz Premagnetization Graph* (SPG). The SPG is very useful

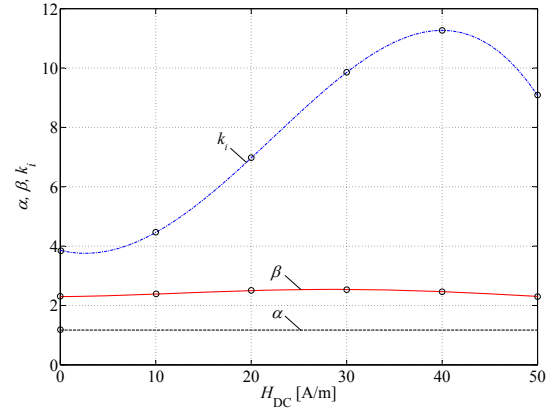


Fig. 9. Steinmetz parameters as a function of premagnetization H_{DC} (ferrite N87), $T = 40^\circ\text{C}$.

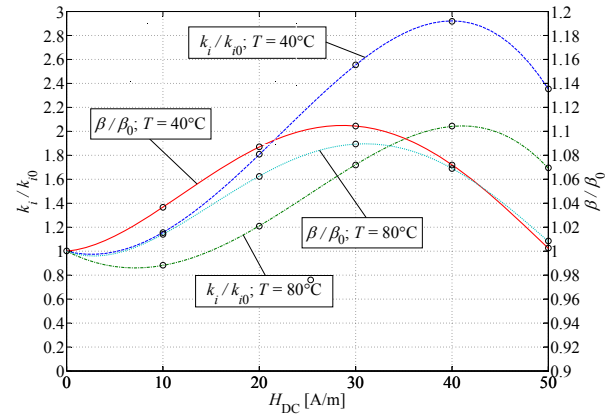


Fig. 10. SPG of the material ferrite N87 (EPCOS).

and it would be valuable to have such a graph in the data sheet of a magnetic material as it would then be possible to calculate core losses under a DC bias condition. Fig. 11 shows how the measured and, based on the SPG, calculated curves compare. For the considered working points the accuracy obtained has always been $\leq \pm 15\%$.

In Appendix A SPGs of other materials (Ferroxcube 3F3 (ferrite), EPCOS N27 (ferrite), and VAC VITROPERM 500F (nanocrystalline material)) are given. Furthermore, a discussion how to extract the Steinmetz parameter value k from the SPG is given in Appendix C. The markers on top of the curves in the SPG represent the Steinmetz parameter values that are directly supported by measurement data. The SPG could be improved by an increase of the H_{DC} resolution to minimize interpolation errors. All given SPGs consider only the premagnetization range where it is still appropriate to use the Steinmetz approach, i.e. the losses still follow a power equation.

In the SPG, the Steinmetz parameters are plotted as a function of H_{DC} . For an ideal toroid H_{DC} can be calculated according to (5) as

$$H_{DC} = \frac{I_{DC} N_1}{l_e}, \quad (13)$$

where I_{DC} is the DC current, N_1 is the number of

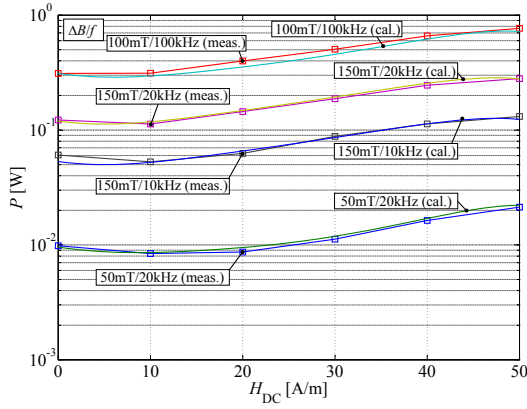


Fig. 11. Core losses under DC bias conditions: measured (meas.) and calculated (cal.) curves (ferrite N87), $T = 40^\circ\text{C}$.

excitation winding turns and l_e the effective magnetic path length of the CUT. It would also be possible to use B_{DC} instead of H_{DC} . For cores without air gaps, H_{DC} has the advantage that it is directly calculable from the current (as it is done in this work). For gapped cores, one would need to set up an accurate reluctance model [26] to calculate H_{DC} inside the core. The relationship $B_{DC}(H_{DC})$ is customarily assumed to be the initial magnetization curve [13].

For the derivation of the SPG the losses are calculated according to (12). For the frequency f the unit Hertz Hz has been used and for the peak-to-peak flux density ΔB the unit Tesla T has been used. Consequently, the SPG is only valid when this set of units is used.

Another interesting fact should be pointed out: also the curves for lower values of H_{DC} that are illustrated in Fig. 8 (including the curve for $H_{DC} = 0$) have not the shape of exact straight lines. This illustrates well the fact that the parameter β is only valid for a limited flux density range (in Fig. 8 the flux densities are plotted over a wide range). Same conclusion could be made for α when the losses are plotted over a wide frequency range. This behavior is a general limitation of the Steinmetz approach.

For the sake of completeness, it should be mentioned again that (1) and (2) are equations to calculate the loss *density*. Consequently, this work does not address how to calculate core losses for cores of different shape. Commonly one divides the core into sections of constant flux densities and calculates the occurring losses in each section [27].

V. INFLUENCE OF TEMPERATURE

For an accurate core calculation, the temperature is another important parameter that considerably influences core losses. In Fig. 12 the losses normalized to losses P_0 at zero premagnetization are given for different temperatures. As can be seen for the material ferrite N87, at higher temperatures the influence of a premagnetization on core losses reduces. The temperature influence is described by extending the SPG to curves of different operating temperatures, as shown in Fig. 10.

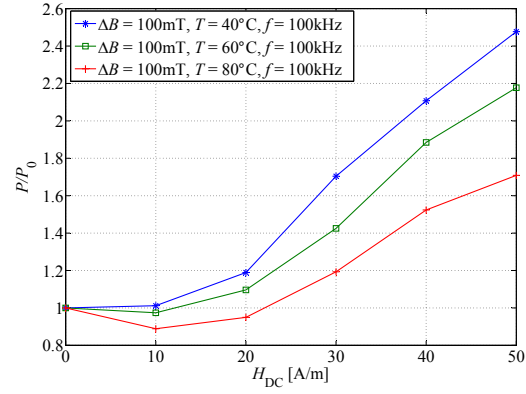


Fig. 12. Core losses under DC bias conditions: measured at different operating temperatures. Normalized to losses P_0 at zero premagnetization. Material N87.

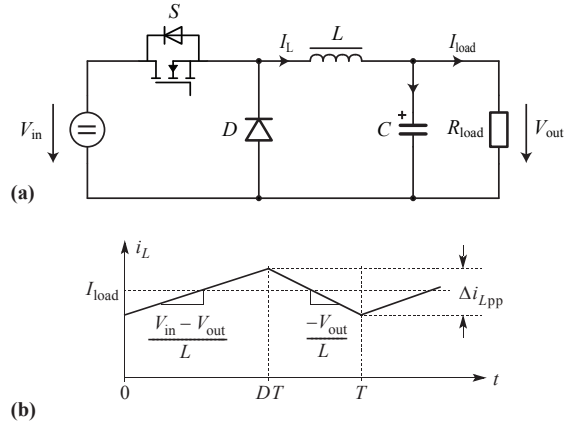


Fig. 13. Buck converter schematic (a) and current waveform (b) with specifications given in Table III.

TABLE III
BUCK CONVERTER SPECIFICATIONS.

V_{in} / V_{out}	12 V / 6 V
f	100 kHz
P	2 W
I_{load}	0.33 A
L	150 μH (EPCOS N87; R25; $N=8$; no air gap) (core part number: B64290L618X87 [23])

VI. EXAMPLE HOW TO USE THE SPG

In the previous sections the SPG has been introduced. This section presents now an easy-to-follow example that illustrates how to calculate core losses of the inductor of a power electronics converter with help of the SPG. In Fig. 13 the schematic and the inductor current waveform of a buck converter, and in Table III the corresponding specifications are given. For the inductor L a DC bias of $H_{DC} = 44 \text{ A/m}$ (according to (13)), and a flux density ripple of $\Delta B = 73 \text{ mT}$ is calculated. The following steps lead to the core losses that occur in the inductor:

- For the used material, the corresponding Steinmetz parameters are extracted from the datasheet. This is

done by solving (1) at three operating points for α , β , and k : $\alpha = 1.25$, $\beta = 2.46$, $k = 15.9$ (values for temperature $T = 40^\circ\text{C}$, at zero premagnetization).

- Next, k_i is calculated according to (3): $k_i = 1.17$.
- k_i and β are now adjusted according to the SPG of the material N87 (cf. Fig. 10) for an operating point with $H_{\text{DC}} = 44 \text{ A/m}$: $k'_i = 2.8 \cdot k_i = 3.28$ and $\beta' = 1.04 \cdot \beta = 2.56$.
- Now, the losses are calculated according to (2). For piecewise linear waveforms, as is the case in the presented example, the integral of (2) may be split into one piece for each linear segment, such that a complicated numerical integration is avoided [10]. The losses follow as

$$\begin{aligned}
 P &= V_e \frac{k'_i (\Delta B)^{\beta' - \alpha}}{T} \\
 &\cdot \left(\left| \frac{\Delta B}{DT} \right|^\alpha DT + \left| \frac{\Delta B}{(1-D)T} \right|^\alpha (1-D)T \right) \\
 &= V_e \frac{k'_i (\Delta B)^{\beta' - \alpha}}{T} \\
 &\cdot \left(\left| \frac{V_{\text{in}} - V_{\text{out}}}{NA_e} \right|^\alpha DT + \left| \frac{-V_{\text{out}}}{NA_e} \right|^\alpha (1-D)T \right) \\
 &= 52.8 \text{ mW}, \tag{14}
 \end{aligned}$$

where $V_e = 3079 \text{ mm}^3$ is the effective core volume, $A_e = 51.26 \text{ mm}^2$ is the effective core cross section, $T = 1/f$ is the period length, and $D = 0.5$ is the duty cycle.

Under the assumption that the Steinmetz parameters had not been adjusted according to the SPG in the example above, the losses would have been calculated as $P = 24.5 \text{ mW}$, which is an underestimation by a factor of more than two.

In case of a load change one has to redo the core loss calculation as a load change leads to a change in the premagnetization and, accordingly, in a change of the core losses. This fact is rarely considered when modeling magnetic components.

VII. CORE LOSSES UNDER DC BIAS CONDITION OF DIFFERENT MATERIALS

Different materials have been tested to gain information how core losses are influenced by a premagnetization in different materials. Measurements on a molypermalloy powder core (Magnetics MPP 300u) and cores of silicon steel (tested: ET165-35 grain-oriented steel with lamination thickness 0.35 mm, M470-50A non-oriented steel with lamination thickness 0.5 mm) have shown that the influence of a premagnetization on losses in these materials is less pronounced. The measurements on the silicon steel cores have been performed up to a DC magnetic field strength just before the core starts to saturate. For very high H_{DC} a small loss increase ($\leq 25\%$) has been observed. The tested powder core (Magnetics MPP 300u; part number: C055433A2) has been tested up to a DC magnetic field strengths of 1200 A/m, up to that operating point the loss change is negligible small.

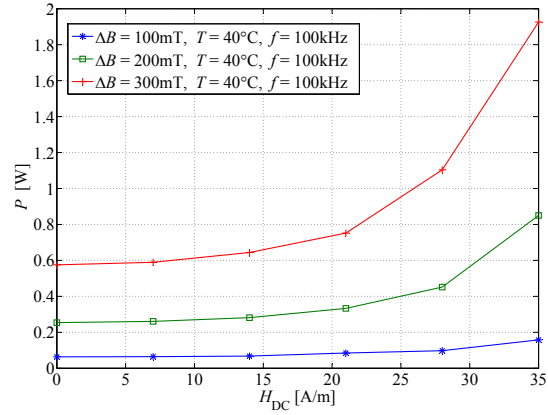


Fig. 14. Core losses under DC bias conditions; material VITROPERM 500F (VAC); core: W452; $f = 100 \text{ kHz}$, $T = 40^\circ\text{C}$.

TABLE IV
IMPACT OF DC BIAS TO CORE LOSSES, AN OVERVIEW OF DIFFERENT MATERIAL CLASSES.

Material Class	Measured Material(s)	Impact on Losses
Soft Ferrites	EPCOS N87, N27, T35 Ferroxcube 3F3	very high
Nanocrystalline	VITROPERM 500F (VAC)	high
Silicon Steel	M470-50A non-oriented steel ET165-35 grain-oriented steel	little
Molypermalloy Powder	Magnetics MPP300	negligible

Losses in the nanocrystalline material VITROPERM 500F from Vacuumschmelze increase under DC bias condition, as can be seen in Fig. 14. The SPGs of the material VITROPERM 500F and of some more ferrites are given in Appendix A. In Table IV an overview of the tested materials is given. The reason for the distinctive behavior of each material class hasn't been studied for this work and could be investigated as part of future work. Tests have been performed only on the above listed components, hence, a general declaration of the whole material class cannot be made with 100% certainty.

VIII. CONCLUSION AND FUTURE WORK

A graph that shows the dependency of the Steinmetz parameters (α , β and k) on premagnetization, i.e. the *Steinmetz Premagnetization Graph* (SPG) has been introduced. Based on the SPG, the calculation of core losses under DC bias condition becomes possible. For the considered frequency range it is shown that the graph is independent of the frequency f . This new approach how to describe losses under DC bias condition is promising due to its simplicity. Such graphs are given for different materials and different operating temperatures.

Furthermore, different material classes have been tested to gain information how core losses are influenced by a premagnetization. Measurements on molypermalloy powder, silicon steel, nanocrystalline material, and ferrite cores have been performed.

For this work, only experiential results have been presented, a material scientific explanation for the distinctive behavior of each material class hasn't been studied and could be investigated as part of future work.

APPENDIX A SPGs OF OTHER MATERIALS

In Fig. 15 the SPG is given for the material EPCOS N27, and in Fig. 16 for the material Ferroxcube 3F3. In Fig. 17 the SPG for the nanocrystalline material VITROPERM 500F from Vacuumschmelze (VAC) is depicted. The independency of the frequency has been confirmed for all materials ($\alpha = \text{constant}$). All given SPGs consider only the premagnetization range where it is still appropriate to use the Steinmetz approach, i.e. the losses still follow a power equation.

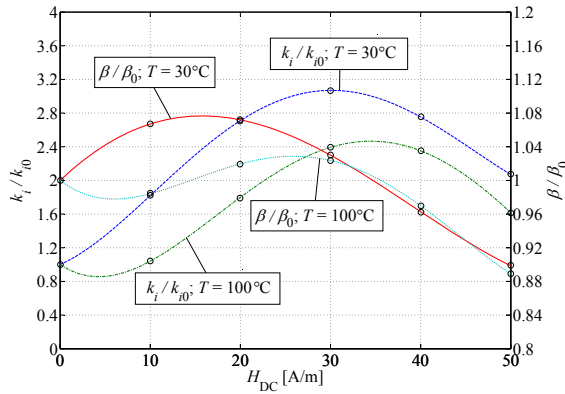


Fig. 15. SPG of the material ferrite N27 (EPCOS); measured on R25 core.

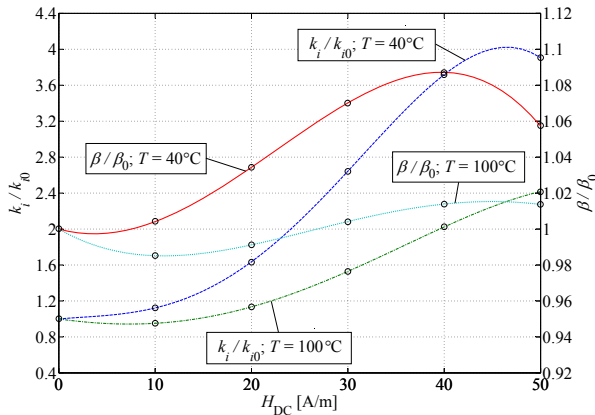


Fig. 16. SPG of the material ferrite 3F3 (Ferroxcube); measured on core type TN25/15/10.

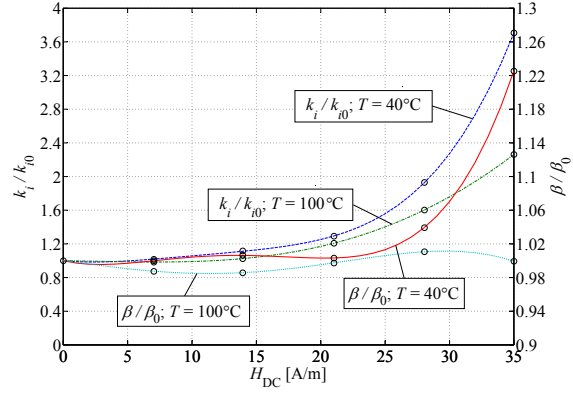


Fig. 17. SPG of the material VITROPERM 500F (VAC); measured on W452 core.

APPENDIX B DERIVATION OF THE STEINMETZ PREMAGNETIZATION GRAPH

The Steinmetz parameters as a function of H_{DC} are described with a fourth order series expansion

$$\begin{bmatrix} \alpha \\ \beta \\ k_i \end{bmatrix} = \begin{bmatrix} \alpha_0 & 0 & 0 & 0 & 0 \\ \beta_0 & p_{\beta 1} & p_{\beta 2} & p_{\beta 3} & p_{\beta 4} \\ k_{i0} & p_{ki1} & p_{ki2} & p_{ki3} & p_{ki4} \end{bmatrix} \cdot \begin{bmatrix} 1 \\ H_{DC} \\ H_{DC}^2 \\ H_{DC}^3 \\ H_{DC}^4 \end{bmatrix} \quad (15)$$

or

$$\mathbf{S} = \mathbf{P} \cdot \mathbf{H}. \quad (16)$$

To extract the dependency of the Steinmetz parameters on the premagnetization, one has to find the right coefficients of the matrix \mathbf{P} . This is an optimization problem. A least square algorithm has been implemented that fits measured curves with calculated data by minimizing the relative error at 3 different values of ΔB , each measured at two frequencies, and 6 premagnetization values H_{DC} (including $H_{DC} = 0$). The losses are calculated according to (12) with Steinmetz parameters from (15)/(16). In the initial matrix \mathbf{P} , all elements p_* (cf. (15)) are set to zero. The values that represent the Steinmetz values under no DC bias condition (α_0 , β_0 , and k_{i0}) have reasonable initial values. As an optimization constraint, it is assumed that $\alpha(H_{DC}) > 1$ and $\beta(H_{DC}) > 2$ for all values of H_{DC} . The optimization is based on the MATLAB function `fminsearch()` that applies the Downhill-Simplex-Approach of Nelder and Mead [28]. This optimization procedure leads to graphs for the Steinmetz dependency as Fig. 9, or normalized to β_0 respectively k_{i0} to the SPG as e.g. shown in Fig. 10.

For the sake of completeness, a drawback of the chosen straightforward fitting procedure is discussed in the following. The above described fitting procedure to calculate the SPG may in some cases result in flawed SPGs that lead to a partly wrong core loss calculation. This is illustrated in Fig. 18, where an initial dip in the k/k_{i0}

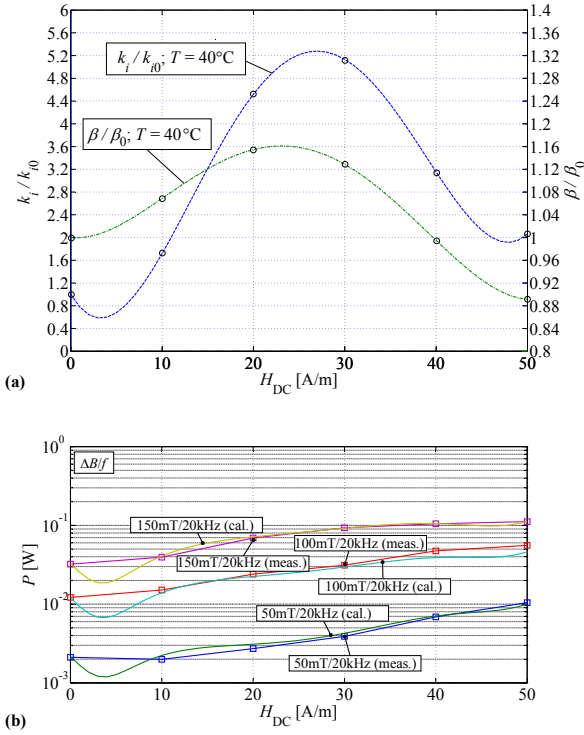


Fig. 18. (a) Illustration of a flawed SPG (material ferrite N27 (EPCOS) at 40°C; measured on R25 core). The initial dip in the curve k/k_{i0} is not supported by measurement data and (b) leads to a partly wrong core loss calculation.

curve (cf. Fig. 18(a)) leads to an underestimation of core losses for very low values of H_{DC} (cf. Fig. 18(b)). This behavior is not supported by any measurement data. Such interpolation errors could e.g. be avoided / limited by an increase of the H_{DC} resolution. However, all published SPGs (except the one in Fig. 18) are tested to be (almost) free from anomalies like that.

APPENDIX C

CLASSIC STEINMETZ PARAMETER k

A short discussion how to extract the Steinmetz parameter value k (not k_i) from the SPG is given in the following. According to (3), for k we have

$$\frac{k}{k_0} = \frac{k_i(2\pi)^{\alpha-1} \int_0^{2\pi} |\cos \theta|^{\alpha} 2^{\beta-\alpha} d\theta}{k_{i0}(2\pi)^{\alpha-1} \int_0^{2\pi} |\cos \theta|^{\alpha} 2^{\beta_0-\alpha} d\theta} \quad (17)$$

that is, under the assumption $\alpha = \text{constant}$,

$$\frac{k}{k_0} = \frac{k_i 2^{\beta}}{k_{i0} 2^{\beta_0}} = \frac{k_i}{k_{i0}} \cdot 2^{(\frac{\beta}{\beta_0}-1)\beta_0}, \quad (18)$$

where β/β_0 can be extracted from the SPG. Of course, it is conceivable to write k/k_0 in the SPG, instead of k_i/k_{i0} . However, because the built test system excites the core with a triangular current shape, k_i/k_{i0} has been chosen for the graph. The iGSE is in any case very broadly used, hence, to avoid further calculations, to have directly the information about k_i is often desired.

REFERENCES

- [1] E. C. Snelling, *Soft Ferrites, Properties and Applications*. 2nd edition, Butterworths, 1988.
- [2] C. P. Steinmetz, "On the law of hysteresis," *Proceedings of the IEEE*, vol. 72, no. 2, pp. 197–221, 1984.
- [3] S. Iyasu, T. Shimizu, and K. Ishii, "A novel iron loss calculation method on power converters based on dynamic minor loop," in *Proc. of European Conference on Power Electronics and Applications*, pp. 2016–2022, 2005.
- [4] T. Shimizu and K. Ishii, "An iron loss calculating method for AC filter inductors used on PWM inverters," in *Proc. of 37th IEEE Power Electronics Specialists Conference (PESC)*, pp. 1–7, 2006.
- [5] K. Terashima, K. Wada, T. Shimizu, T. Nakazawa, K. Ishii, and Y. Hayashi, "Evaluation of the iron loss of an inductor based on dynamic minor characteristics," in *Proc. of European Conference on Power Electronics and Applications*, pp. 1–8, 2007.
- [6] G. Bertotti, *Hysteresis in Magnetism*. Academic Press, Inc., 1998.
- [7] W. A. Roshen, "A practical, accurate and very general core loss model for nonsinusoidal waveforms," *IEEE Transactions on Power Electronics*, vol. 22, no. 1, pp. 30–40, 2007.
- [8] J. Reinert, A. Brockmeyer, and R. De Doncker, "Calculation of losses in ferro- and ferrimagnetic materials based on the modified Steinmetz equation," *IEEE Transactions on Industry Applications*, vol. 37, no. 4, pp. 1055–1061, 2001.
- [9] J. Li, T. Abdallah, and C. R. Sullivan, "Improved calculation of core loss with nonsinusoidal waveforms," in *Industry Applications Conference, 2001. 36th IEEE IAS Annual Meeting.*, vol. 4, pp. 2203–2210, 2001.
- [10] K. Venkatachalam, C. R. Sullivan, T. Abdallah, and H. Tacca, "Accurate prediction of ferrite core loss with nonsinusoidal waveforms using only Steinmetz parameters," in *Proc. of IEEE Workshop on Computers in Power Electronics*, pp. 36–41, 2002.
- [11] J. Biela, U. Badstuebner, and J. W. Kolar, "Impact of power density maximization on efficiency of DC-DC converter systems," *IEEE Transactions on Power Electronics*, vol. 24, pp. 288–300, Jan. 2009.
- [12] I. Villar, U. Viscarret, I. Etxeberria-Otadui, and A. Rufer, "Global loss evaluation methods for nonsinusoidally fed medium-frequency power transformers," *IEEE Transactions on Industrial Electronics*, vol. 56, pp. 4132–4140, Oct. 2009.
- [13] G. Niedermeier and M. Esguerra, "Measurement of power losses with DC-bias - The Displacement Factor," in *Proc. of PCIM*, pp. 169–174, 2000.
- [14] A. Brockmeyer, "Experimental evaluation of the influence of DC-premagnetization on the properties of power electronic ferrites," in *Proc. of the 11th Annual Applied Power Electronics Conference (APEC)*, vol. 1, pp. 454–460, 3–7 March 1996.
- [15] T. Komma, *Allgemein gültiger Entwurfsalgorithmus für magnetische Komponenten in Schaltnetzteilen mit unterschiedlichen Topologien und Schaltfrequenzen bis 2 MHz*. PhD thesis, Technische Universität Dresden, 2005.
- [16] M. S. Lancarotte, C. Goldemberg, and A. A. Pentead, "Estimation of FeSi core losses under PWM or DC bias ripple voltage excitations," *IEEE Transactions on Energy Conversion*, vol. 20, no. 2, pp. 367–372, 2005.
- [17] C. A. Baguley, B. Carsten, and U. K. Madawala, "The effect of DC bias conditions on ferrite core losses," *IEEE Transactions on Magnetics*, vol. 44, pp. 246–252, Feb. 2008.
- [18] C. A. Baguley, U. K. Madawala, and B. Carsten, "A new technique for measuring ferrite core loss under DC bias conditions," *IEEE Transactions on Magnetics*, vol. 44, no. 11, pp. 4127–4130, 2008.
- [19] B. Carsten, "Why the magnetics designer should measure core loss; with a survey of loss measurement techniques and a low cost, high accuracy alternative," in *Proc. of PCIM*, pp. 163–179, 1995.
- [20] F. Dong Tan, J. Vollin, and S. Cuk, "A practical approach for magnetic core-loss characterization," *IEEE Transactions on Power Electronics*, vol. 10, pp. 124–130, Mar. 1995.
- [21] W. Shen, F. Wang, D. Boroyevich, and C. W. Tipton, "Loss characterization and calculation of nanocrystalline cores for high-frequency magnetics applications," *IEEE Transactions on Power Electronics*, vol. 23, pp. 475–484, Jan. 2008.
- [22] V. Thottuvelil, T. Wilson, and H. Owen, "High-frequency measurement techniques for magnetic cores," *IEEE Transactions on Power Electronics*, vol. 5, pp. 41–53, Jan. 1990.
- [23] *Ferrites and Accessories, Edition 2007*. EPCOS AG.

- [24] M. Mu, Q. Li, D. Gilham, F. C. Lee, and K. D. T. Ngo, "New core loss measurement method for high frequency magnetic materials," in *Proc. of IEEE Energy Conversion Congress and Exposition (ECCE)*, pp. 4384–4389, 2010.
- [25] A. V. den Bossche and V. C. Valchev, *Inductors and Transformers for Power Electronics*. CRC Press, Taylor & Francis Group, 2005.
- [26] J. Mühlethaler, J. W. Kolar, and A. Ecklebe, "A novel approach for 3D air gap reluctance calculations," in *Proc. of the 8th International Conference on Power Electronics - ECCE Asia*, pp. 446–452, 2011.
- [27] J. Mühlethaler, J. W. Kolar, and A. Ecklebe, "Loss modeling of inductive components employed in power electronic systems," in *Proc. of the 8th International Conference on Power Electronics - ECCE Asia*, pp. 945–952, 2011.
- [28] J. A. Nelder and R. Mead, "A simplex method for function minimization," *The Computer Journal*, vol. 4, pp. 308–313, 1965.



Jonas Mühlethaler (S'09) received his M.Sc. degree in electrical engineering from the Swiss Federal Institute of Technology (ETH) Zurich, Zurich, Switzerland, in 2008. During his studies, he focused on power electronics and electrical machines. In his M.Sc. thesis, which he wrote at ABB Corporate Research in Sweden, he worked on compensating torque pulsation in Permanent Magnet Motors. Since 2008 he is working toward the Ph.D. degree in the Power Electronic Systems Laboratory, focusing on modeling and designing magnetic components.



Juergen Biela (S'04 M'06) received the Diploma (with honors) from Friedrich-Alexander University (FAU) Erlangen, Nuremberg, Germany, in 1999 and the Ph.D. degree from the Swiss Federal Institute of Technology (ETH) Zurich, Zurich, Switzerland, in 2006. During his studies, he dealt in particular with resonant dc-link inverters at Strathclyde University, Glasgow, U.K., and the active control of series-connected IGCTs at the Technical University

of Munich, München, Germany. From 2000, he was with the Research Department of A&D Siemens, Germany, where he worked on inverters with very high switching frequencies, SiC components, and EMC. In July 2002, he was with the Power Electronic Systems Laboratory (PES), ETH Zurich, while working toward the Ph.D. degree, focusing on optimized electromagnetically integrated resonant converter. From 2006 to 2007, he was a Postdoctoral Fellow with PES and has been a Guest Researcher at the Tokyo Institute of Technology, Tokyo, Japan. From 2007 to mid 2010, he was a Senior Research Associate with PES. In August 2010, he was appointed Associate Professor and Head of the Laboratory for High Power Electronic Systems at ETH Zurich. His current research is focused on design, modeling, and optimization of PFC, dc-dc, and multilevel converters with emphasis on SMART Grid, electric mobility and traction applications as well as pulsed-power systems for medical and accelerator applications.



Johann W. Kolar (F'10) received his M.Sc. and Ph.D. degree (summa cum laude / promotio sub auspiciis praesidentis rei publicae) from the University of Technology Vienna, Austria. Since 1984 he has been working as an independent international consultant in close collaboration with the University of Technology Vienna, in the fields of power electronics, industrial electronics and high performance drives. He has proposed numerous novel converter topologies and modulation/control concepts, e.g., the VIENNA Rectifier, the Swiss Rectifier, and the three-phase AC-AC Sparse Matrix Converter. Dr. Kolar has published over 400 scientific papers in international journals and conference proceedings and has filed more than 80 patents. He was appointed Professor and Head of the Power Electronic Systems Laboratory at the Swiss Federal Institute of Technology (ETH) Zurich on Feb. 1, 2001. The focus of his current research is on AC-AC and AC-DC converter topologies with low effects on the mains, e.g. for data centers, More-Electric-Aircraft and distributed renewable energy systems, and on Solid-State Transformers for Smart Microgrid Systems. Further main research areas are the realization of ultra-compact and ultra-efficient converter modules employing latest power semiconductor technology (SiC and GaN), micro power electronics and/or Power Supply on Chip Systems, multi-domain/scale modeling/simulation and multi-objective optimization, physical model-based lifetime prediction, pulsed power, and ultra-high speed and bearingless motors. He received the Best Transactions Paper Award of the IEEE Industrial Electronics Society in 2005, the Best Paper Award of the ICPE in 2007, the 1st Prize Paper Award of the IEEE IAS IPCC in 2008, the IEEE IECON Best Paper Award of the IES PETC in 2009, the 2009 IEEE Power Electronics Society Transaction Prize Paper Award and the 2010 Best Paper Award of the IEEE/ASME Transactions on Mechatronics. He also received an Erskine Fellowship from the University of Canterbury, New Zealand, in 2003. He initiated and/or is the founder/co-founder of 4 spin-off companies targeting ultra-high speed drives, multi-domain/level simulation, ultra-compact/efficient converter systems and pulsed power/electronic energy processing. In 2006, the European Power Supplies Manufacturers Association (EPSMA) awarded the Power Electronics Systems Laboratory of ETH Zurich as the leading academic research institution in Power Electronics in Europe. Dr. Kolar is a Fellow of the IEEE and a Member of the IEEEJ and of International Steering Committees and Technical Program Committees of numerous international conferences in the field (e.g. Director of the Power Quality Branch of the International Conference on Power Conversion and Intelligent Motion). He is the founding Chairman of the IEEE PELS Austria and Switzerland Chapter and Chairman of the Education Chapter of the EPE Association. From 1997 through 2000 he has been serving as an Associate Editor of the IEEE Transactions on Industrial Electronics and since 2001 as an Associate Editor of the IEEE Transactions on Power Electronics. Since 2002 he also is an Associate Editor of the Journal of Power Electronics of the Korean Institute of Power Electronics and a member of the Editorial Advisory Board of the IEEEJ Transactions on Electrical and Electronic Engineering.



Andreas Ecklebe (M'07) received the Dipl.-Ing. degree in electrical engineering in 2002 and the Dr.-Ing. degree in electrical engineering in 2009 both from the Otto-von-Guericke University, Magdeburg. From 2002 to 2004 he was with SMS Demag AG and Alstom Power Conversion, where he was engaged in the design of technological control systems for large scale industrial automation solutions. Since 2008 he is with ABB Corporate Research, Baden-Daettwil, Switzerland, where he is currently leading the Power Electronics Integration Research Group.